Electrically tunable multicolored filter using birefringent plasmonic resonators and liquid crystals – Supporting Information

Luc Driencourt,[†] Franois Federspiel,[‡] Dimitrios Kazazis,[¶] Li-Ting Tseng,[¶] Richard Frantz,[‡] Yasin Ekinci,[¶] Rolando Ferrini,[†] and Benjamin Gallinet[*,†]

†*CSEM Muttenz, Tramstrasse 99, CH-4132 Muttenz*

‡*Rolic Technologies Ltd., Allschwil, Switzerland*

¶*Paul Scherrer Institut (PSI), Villigen, Switzerland*

E-mail: benjamin.gallinet@csem.ch

Oscillator model

The optical response of the plasmonic resonators can be modeled with the response of a forced harmonic oscillator with resonance frequency ω_0 and γ_0, parameters depending on the geometry of the nanostructure and plasma frequency of the material. The amplitude and phase of the oscillator are respectively given by:

$$I(\omega) = |c(\omega)|^2 \,, \tag{1}$$

and

$$\phi(\omega) = \arg(c(\omega)) \,, \tag{2}$$

where

$$c(\omega) = \frac{f\gamma_0\omega_0}{\omega_0^2 - \omega^2 + i\gamma_0\omega_0} \,, \tag{3}$$

and f is proportional to the force amplitude. The plasmonic nanostructure is assumed to be an infinite array of individual resonators interacting with TM–polarized light, while the TE–polarized has a constant transmission T_{TE} of 1. At resonance, the field is scattered in reflection, so that the transmitted field intensity in TM polarization is given by:

$$T_{\mathrm{TM}}(\omega) = 1 - A(\omega) \,. \tag{4}$$

Figure S1a shows the TE and TM polarized transmission modeled using Eq. (4). In a realistic system, the phase response does not undergo a full phase shift of π across the resonance (Fig. S1), and we therefore assume to have a total phase shift given by the phenomenological parameter η_0. The phase delay for low wavelengths between the TE and TM polarized light is also assumed to be 0, so that the wavelength–dependent phase delay ϕ_T between the TE

and TM polarized light satisfies the following function of the wavelength:

$$\Delta\phi(\omega) = \pi + \eta_0\phi(\omega)\,. \tag{5}$$

In Fig. S1b, the phase shift is calculated using Eq. (5) and the parameter η_0 is chosen so that its amplitude for high wavelength matches the ellipsometric measurement of Fig. S2a. The spectrum of the transmitted light under crossed polarization is strongly influenced by the amplitude of the phase shift η_0.

A Jones–matrix calculation of the light intensity transmitted through a system between a polarizer at 45° and a rotating analyzer with orientation θ yields for the transmitted amplitude:[1]

$$T_{\text{out}} = \begin{pmatrix} \cos^2\theta & -\sin\theta\cos\theta \\ -\sin\theta\cos\theta & \sin^2\theta \end{pmatrix} \cdot \begin{pmatrix} \sqrt{T_{\text{TM}}}e^{i\Delta\phi} & 0 \\ 0 & \sqrt{T_{\text{TE}}} \end{pmatrix} \begin{pmatrix} 1/\sqrt{2} \\ 1/\sqrt{2} \end{pmatrix}, \tag{6}$$

and the transmitted intensity:

$$|T_{\text{out}}|^2 = T_{\text{TM}}\cos^2\theta/2 + T_{\text{TE}}\sin^2\theta/2 + T_{\text{TM}}T_{\text{TE}}\cos(\Delta\phi)\cos(\theta)\sin(\theta)\,. \tag{7}$$

Figures S1c and S1d show an oscillator model of the nanostructure with resonance parameters extracted from optical measurements of the transmission amplitude and phase retardation. In particular, by comparing Figures 1c and d, it can be observed that the modulation amplitude of the spectral response between crossed polarizers strongly depends on the amplitude of the phase retardation (red and cyan colors for $\theta = 45°$ and $\theta = 135°$, respectively).

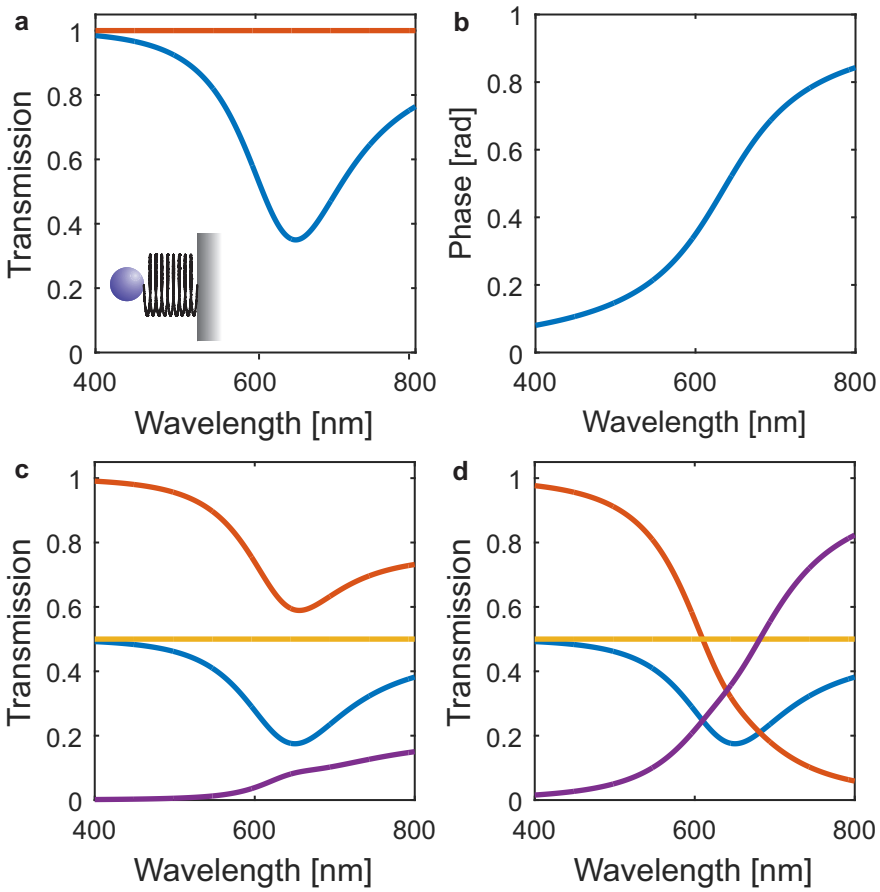

Figure S1: **Harmonic oscillator model**. (a) Transmission of TE (red) and TM (blue) polarized light (parameters $\lambda_0 = 2\pi c/\omega_0 = 640$nm and $\gamma_0 = 0.25\omega_0$). (b) Phase delay between TE and TM polarized light (with η_0=0.32). c–d) Transmission through a system of polarizers following Eq. (7) as a function of the rotation angle of the analyzing polarizer θ with (c) η_0=0.32 (c) η_0=1. Blue–$\theta = 0$, violet–$\theta = 45°$, yellow–$\theta = 90°$, red–$\theta = 135°$

Resonance–induced colors

In this section, the colors observed in transmission through the plasmonic nanostructure are discussed in more details, with support of semi–analytical and numerical models. The CIE gamut spanned by the nanostructure between crossed polarizers can be reconstructed from experimental transmission measurement at TM and TE polarization and the phase retardation measured by ellipsometry. Using Jones matrices, the transmitted intensity is

given by:

$$|T_{\text{out}}|^2 = T_{\text{TM}}^2 \cos^2\theta/2 + T_{\text{TE}}^2 \sin^2\theta/2 + T_{\text{TM}} T_{\text{TE}} \cos(\Delta\phi) \cos\theta \sin\theta\,. \tag{8}$$

where $\Delta\phi$ is the phase retardation measured by ellipsometry and T_{TM} and T_{TE} are the measured transmittance coefficients when the $\theta = \pi/2$ and 0, respectively. The related spectra and CIE color plot are given in Fig. S2.

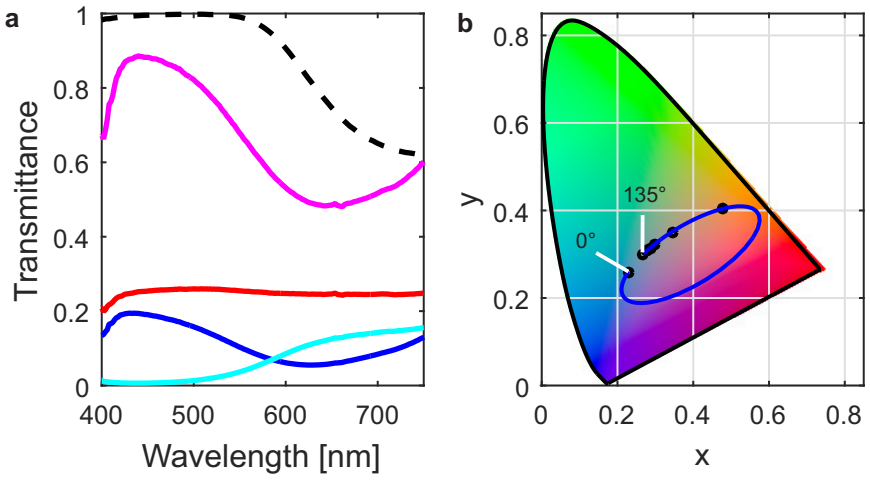

Figure S2: **Reconstruction of plasmon–induced colors.** (a) Dashed line: $\cos(\Delta\phi)$ with $\Delta\phi$ measured by ellipsometry. Red-$\theta = 0$, purple-$\theta = \pi/4$, blue-$\theta = \pi/2$, cyan-$\theta = 3\pi/4$. (b) CIE plot for spectra corresponding to the angles in Figure 2 of the main text.

It can be seen that the reconstructed spectra and colors as a function of the analyzer angle are well reconstructed using Eq. (8), thus validating the model of Eq. (8).

Numerical simulations of the transmission through the nanostructure have been performed with rigorous coupled wave analysis using 60 Fourier harmonics[2] with experimental values of the silver permittivity.[3] The silver structures are completely surrounded by a homogeneous medium with the permittivity of Ormocomp. The imaginary part of the silver permittivity has been multiplied by 2 in order to model fabrication imperfections. The results are shown in Fig. S3, from where a good spectral agreement with experimental measurements can be observed.

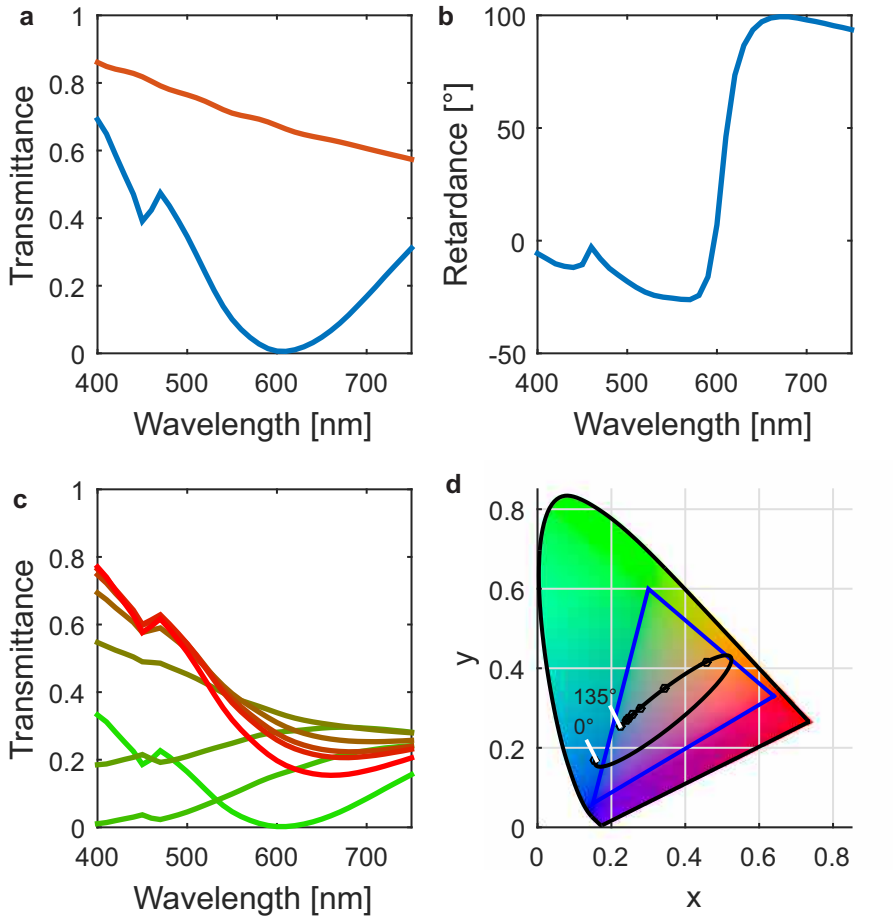

Figure S3: Numerical simulations. (a) Transmission with TM and TE polarization. (b) Phase retardation between TM and TE polarization. (c) Transmission through a system of polarizers following Eq. (8) as a function of the rotation angle of the analyzing polarizer θ, for analyzer angles corresponding to Fig. 2f. (d) Corresponding CIE color plot.

The numerical model has been used to optimize the nanostructure parameters as shown in Fig. S4. The period has been determined in order to minimize angular dependance of the optical properties (Fig. S4a), that is below 180nm, while still maximizing the feature size for manufacturability. As can be observed in Fig. S4b, increasing the wire width ref shifts and broadens the plasmon resonance, which is an effect of neighbor–to–neighbor coupling.[4] The width of 105nm has been chosen to minimize this broadening while maximizing the feature size for manufacturability.

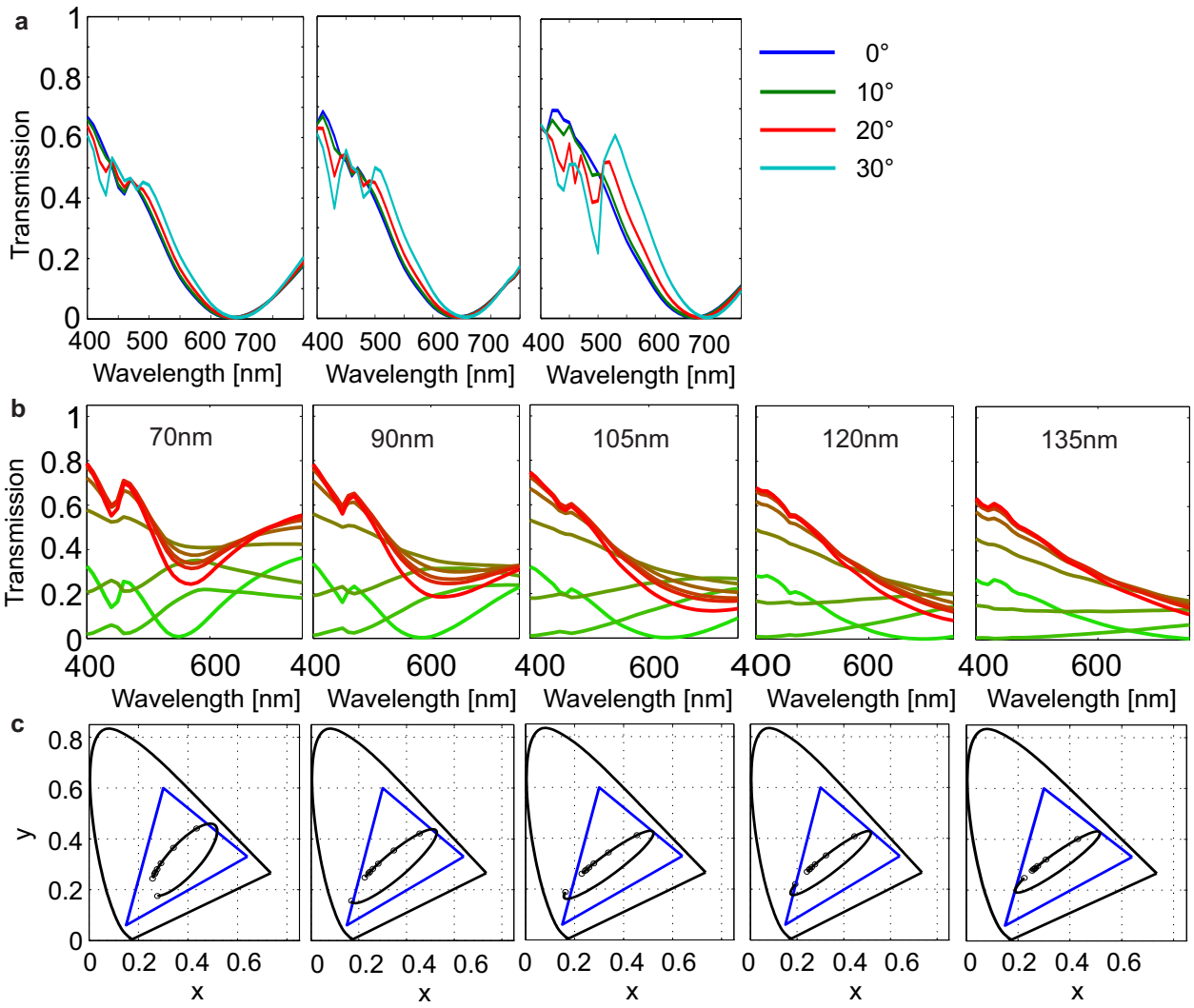

Figure S4: Optimization of grating profile. (a) TM polarized transmission for periods 160nm, 180nm and 200nm as a function of incident wavelength and angle. The silver thickness is 20nm and the size of the silver wires is 70% of the period. (b) Polarized transmittance for analyzer angles corresponding to Fig. 2f for different nanowire sizes. The period is 160nm and the silver thickness is 20nm. (c) Corresponding CIE color plot.

Finally, the film thickness has been chosen in order to maximize the color gamut and peak transmission. As can be seen in Fig. S5, a film thickness in the range between 20nm and 30nm can be chosen.

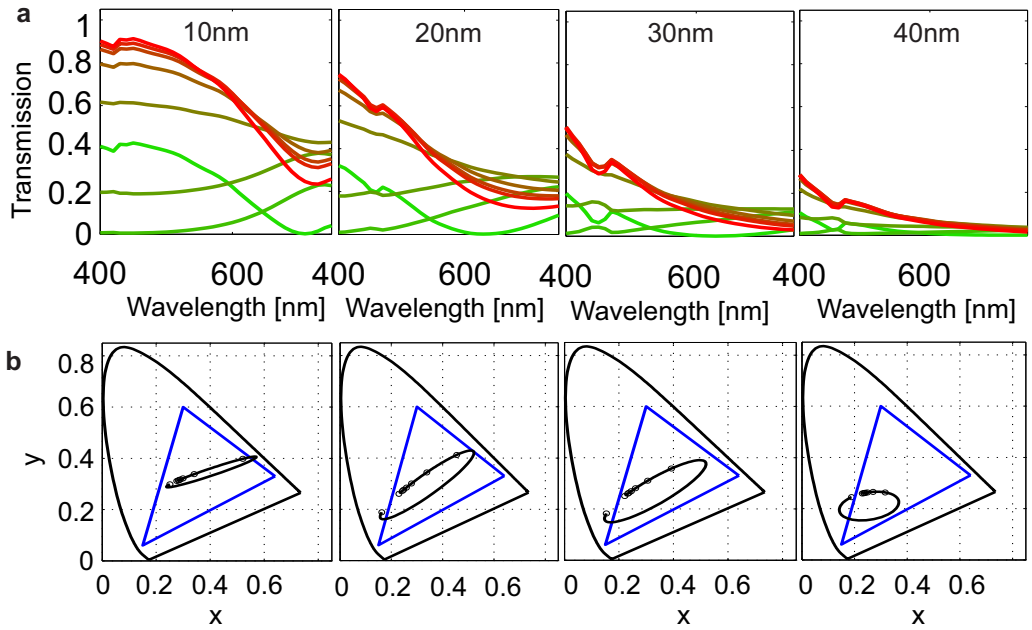

Figure S5: Optimization of film thickness. (a) Polarized transmittance for analyzer angles corresponding to Fig. 2f for different silver film thicknesses. The period is 160nm and the silver wire width is 110nm. (b) Corresponding CIE color plot.

The transmission spectra T^2_{TM} and T^2_{TE} of the nanostructure as a function of the incidence angle in incidence planes across and along the grating lines has been measured, for both polarizations respectively. The results are shown in Fig. S6.

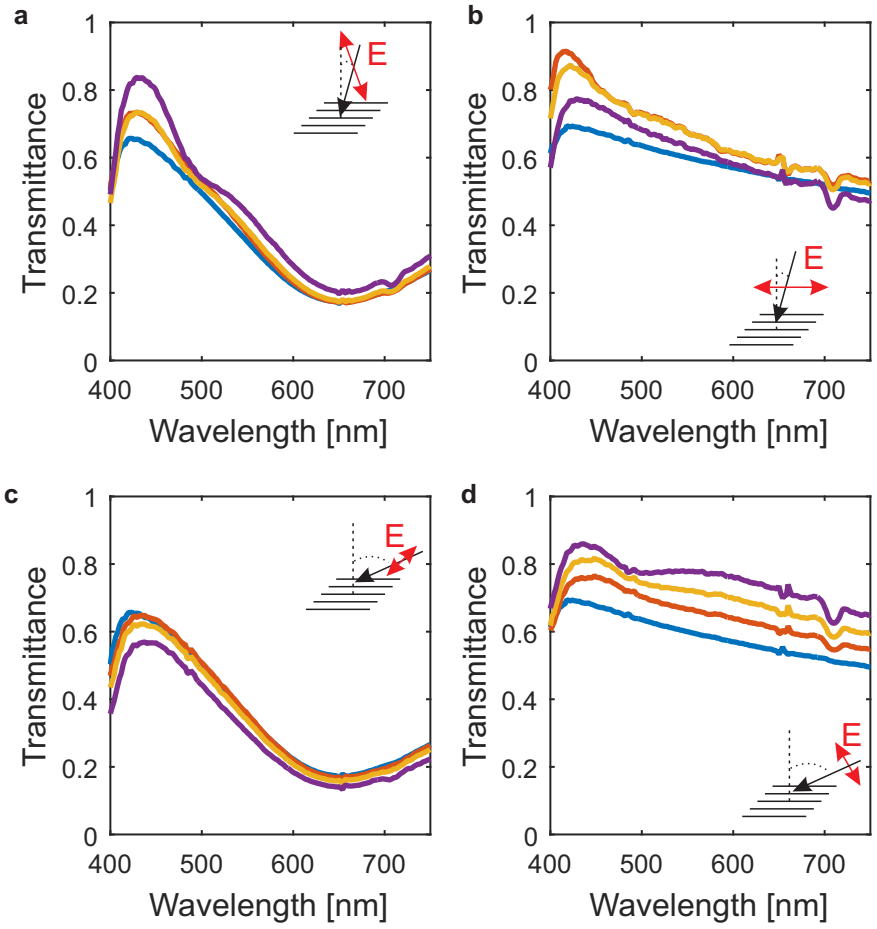

Figure S6: Angular dependence of plasmon resonance in the nanostructure. The transmittance is measured for both polarizations along two incidence planes. Blue–normal incidence, red–15°, yellow–30°, purple–45°.

Overall, a very good stability of the spectral lineshape is observed up to 45° tilt, regardless of the polarization and incidence plane. This is due to the fact that the periodicity of the metallic lines is 160nm, i.e. deep sub–wavelength, thus avoiding dispersive effects. The plasmonic device has therefore a broad angular stability, which can be an asset for its integration in optoelectronic devices. The modulation of the transmission for TM polarization corresponding to the resonance ranges from 20% to above 60%.

Full system spectral reconstruction

This section aims at validating the model of the Jones Matrices used to describe the optical properties of the tunable filter system. To this end, optical measurements of the different components will be incorporated in the model to reconstruct the transmission measurements of the system as a function of the voltage applied to the LCC. The intensity of the transmitted field can be modeled as:

$$|T_{\text{out}}|^2 = \frac{[T_{\text{TM}}\cos(\delta/2)]^2}{2} + \frac{[T_{\text{TE}}\sin(\delta/2)]^2}{2} + T_{\text{TM}}T_{\text{TE}}\cos(\Delta\phi)\cos(\delta/2)\sin(\delta/2)\,, \quad (9)$$

where δ is the phase delay induced by the voltage–dependent birefringence $\Delta n(V)$ in the liquid crystal material of thickness t:

$$\delta = \frac{2\pi\Delta n(V)t}{\lambda}\,. \quad (10)$$

Considering a wavelength dependence of the retardation δ following Eq. (10), the factors $\cos(\delta/2)$ and $\sin(\delta/2)$ of Eq. (9) generate additional colors which are combined with the contribution T_{TM}, T_{TE} and $\Delta\Phi$ of the plasmonic nanostructure. These quantities can be directly accessed by measuring the transmission of the LCC in the configuration of Fig. S7a, replacing the plasmonic nanostructure and the entrance polarizer by a polarizer at three different orientations. For 0°, Eq. (9) becomes $I_{\text{out}} = \cos(\delta/2)^2$, with corresponding transmission shown in Fig. S6c as a function of the applied voltage and the corresponding colors in Fig. S7d. For 90°, Eq. (9) becomes $I_{\text{out}} = \sin(\delta/2)^2$ (Fig. S7e, with corresponding colors in Fig. S7f). The measurement of the cross term $\cos(\delta/2)\sin(\delta/2)$ can be performed with the entrance polarizer oriented at ±45° knowing the coefficients $\cos(\delta/2)^2$ and $\sin(\delta/2)^2$ (Fig. S7b). The measurements in Fig. S7 are normalized to the intensity transmitted by the entrance polarizer only.

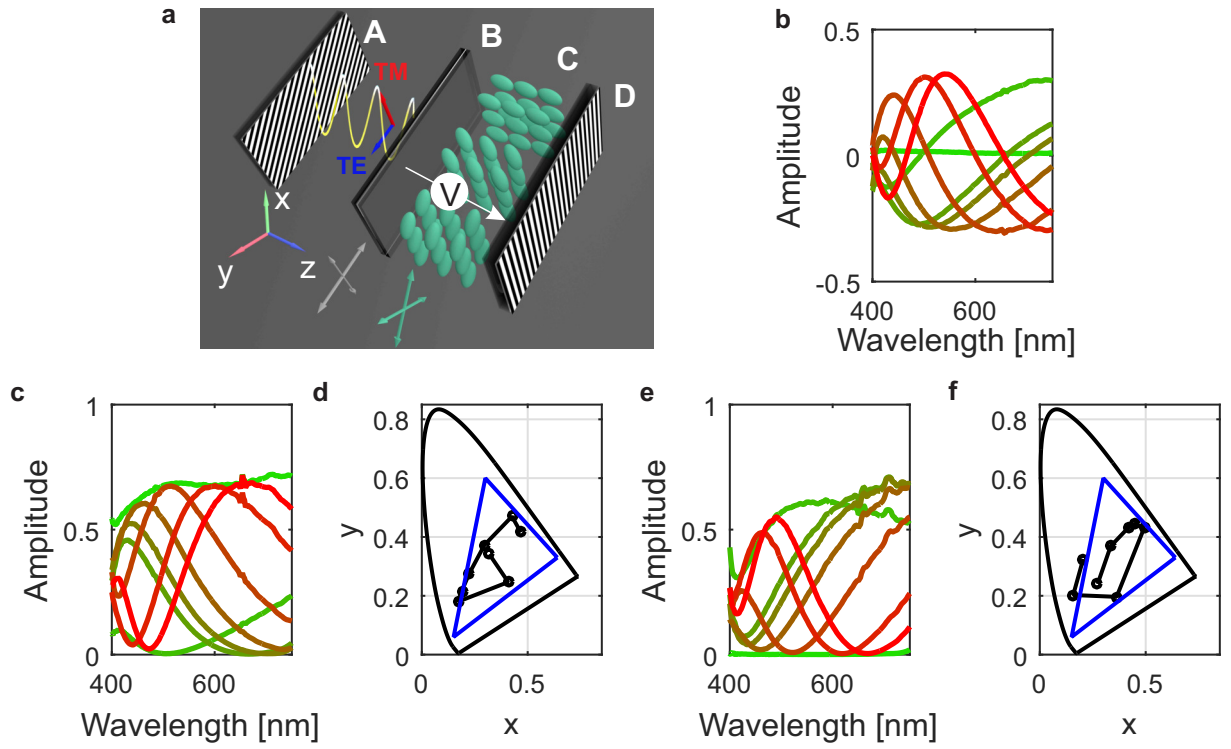

Figure S7: **Birefringence–induced colors.**(a) Measurement setup including (A) an entrance polarizer and the voltage–tunable polarisation analyzer comprising (B) a quarter waveplate, (C) a liquid crystal cell (LCC) with main retardation axes rotated by 45° from the main retardation axes of the waveplate, and (E) a polarizer with fixed orientation. The entrance polarizer can be oriented at 0°, ±45° or 90° compared to the exit polarizer. (b) Amplitude spectrum of $\cos(\delta/2)\sin(\delta/2)$. (c) Amplitude spectrum of $\cos(\delta/2)^2$ and (d) corresponding CIE color plot. (e) Amplitude spectrum of $\sin(\delta/2)^2$ and (f) corresponding CIE color plot. The applied voltages are green–2V to red–6.5V, with 3.15V, 3.45V, 3.55V, 3.75V, 4.2V and 5.25V as intermediate values.

On the other hand, the coefficients T_{TM}, T_{TE} related to the plasmonic nanostructure are extracted from the transmittance measurements of Fig. S6. The phase retardation is measured by ellipsometry (Fig. 2 of the main text). When combined together with the voltage–dependent coefficients from the LCC, the intensity transmitted through the full system $|T_{\mathrm{out}}|^2$ can be reconstructed using Eq. (9) (Fig. S8). An additional degree of tunability of the color range is related to the rotation with angle ϕ of the LCC relative to the plasmonic

nanostructure and the entrance polarizer, which can be written directly as:

$$\begin{pmatrix} T'_{\mathrm{TM}} \\ T_{\mathrm{TE}} \end{pmatrix} = \begin{pmatrix} \cos\psi & \sin\psi \\ -\sin\psi & \cos\psi \end{pmatrix} \cdot \begin{pmatrix} T_{\mathrm{TM}} \\ T_{\mathrm{TE}} \end{pmatrix} . \tag{11}$$

In Fig. S8a, the spectrum of the liquid crystal cell alone with an entrance polarizer at 45° is reconstructed, corresponding to $\Delta\phi = 0$, $T_{\mathrm{TM}} = T_{\mathrm{TE}} = 1/\sqrt{2}$. The cases of Fig. S8b and c correspond to $\psi = 4°$ and $\psi = -45°$, respectively, with the aim of enhancing the green and red colors, respectively.

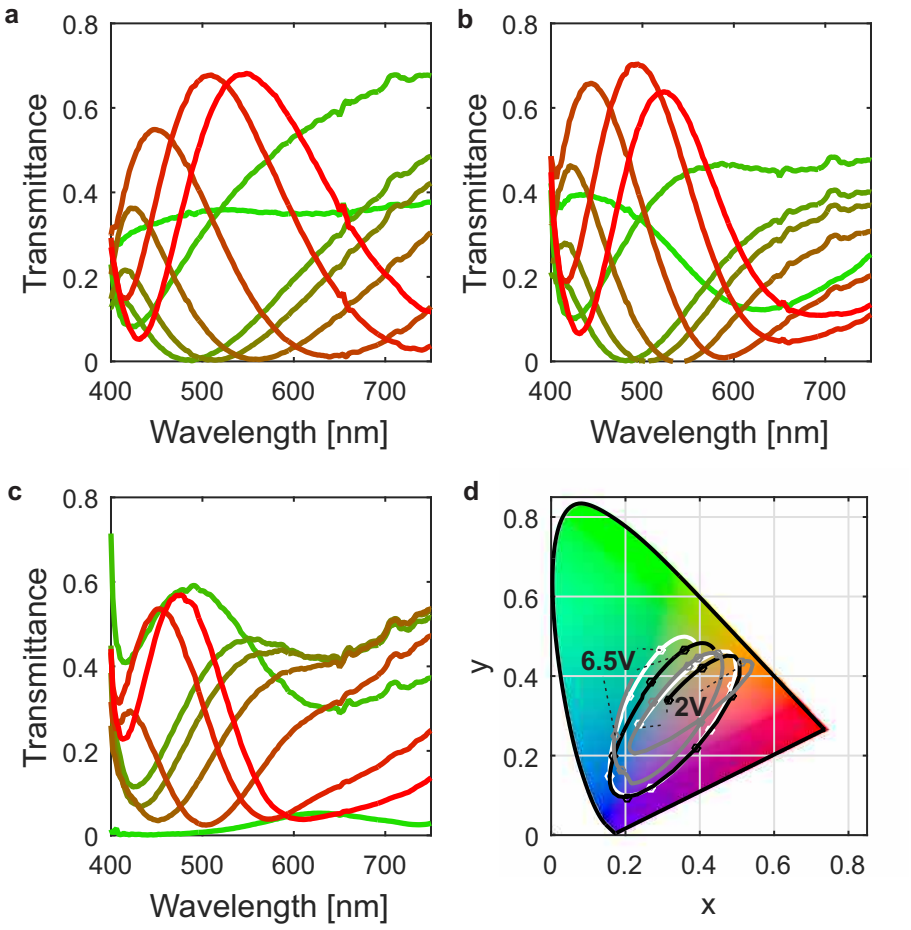

Figure S8: **Reconstruction of color transmitted through the tunable filter.** (a) Liquid crystal cell only. (b) With plasmonic nanostructure oriented at $\psi = 4°$. (c) With plasmonic nanostructure oriented at $\psi = -45°$. (d) Corresponding CIE color plot with configurations of panel a (black), panel b (white) and panel c (gray). The applied voltages are green–2V to red–6.5V, with 3.15V, 3.45V, 3.55V, 3.75V, 4.2V and 5.25V as intermediate values.

Overall, the reconstructed spectra and colors agree well with the measurements reported in the main text for all three configurations. All features can be reproduced, which validates the model. In particular, the model can predict the enhancement of the green and red colors by the nanostructure and can be used as a design tool for the nanostructure element.

Construction of input polarizer with multiple orientations

An input polarizer with 16 different orientations has been realized from a high resolution picture of a chameleon. A map of the different orientations is shown in Fig. S9. The light transmitted through the patterned polarizer and the nanostructure reaches the polarization analyzer with different combinations of TM–, TE– and elliptically polarized light. As an effect, different color ranges and different permutations of the colors as a function of the applied voltage are obtained, resulting in colorful chameleon images such as shown in the main text.

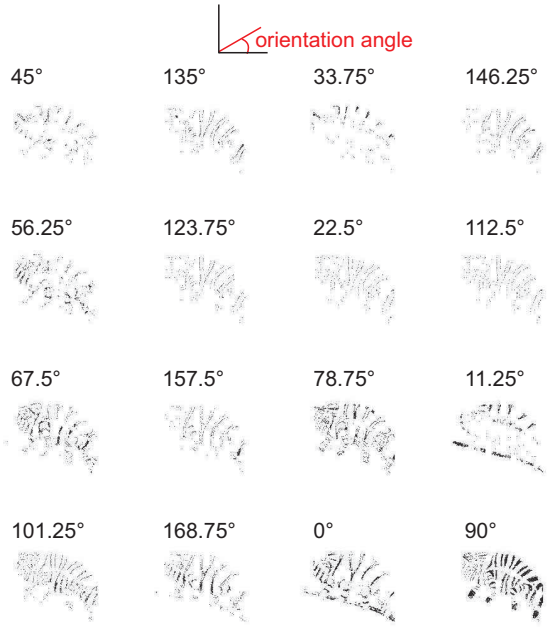

Figure S9: Orientation map of the patterned polarizers. Black areas are oriented at the angle specified in the inset with 0° corresponding to an horizontal orientation.

Filter configuration for image acquisition

For the color image acquisition, the tunable filter had a configuration which balances the three primary colors, with an angle $\psi = 7°$ in Eq. (11). Images of the color checker have been acquired at three different voltages, corresponding to the primary colors. The transmission spectra at these voltages have been measured and are reported in Fig. S10.

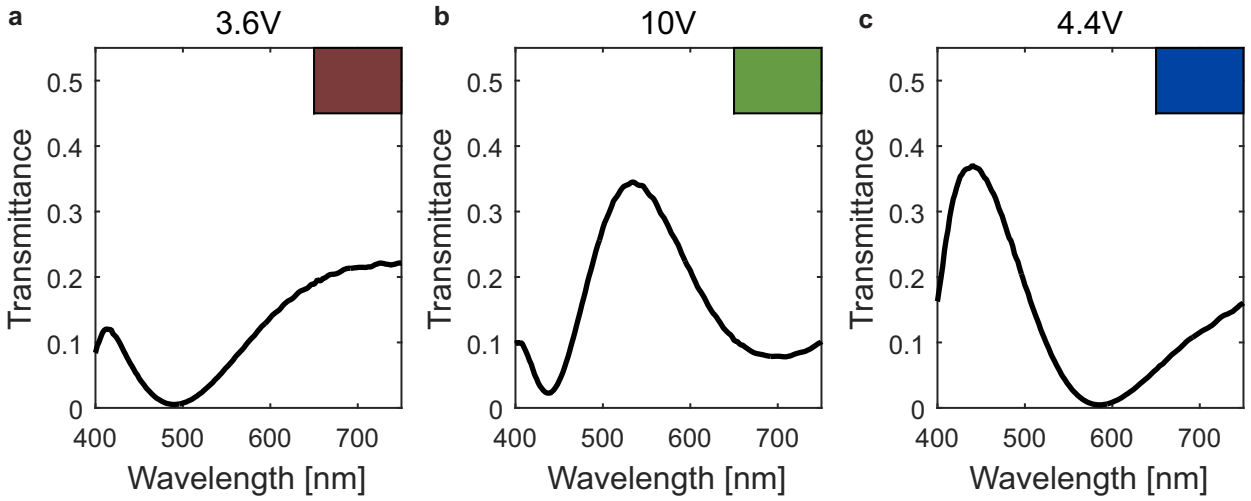

Figure S10: **Filter configuration for image acquisition.** Transmission spectra at voltages corresponding to (a) Red, (b) Green, (c) Blue. The corresponding colors are shown in the inset.

In this configuration, the saturation of the red color has been increased and the voltage required to obtain a saturated green is increased to 10V.

Photographs

Photographs of the homogeneous device with and without the plasmonic nanostructure are shown in Fig. S11 at different voltages. Its lateral dimension is 20mm. The configurations of Fig. S11a and Fig. S11b correspond to Fig. 3a and 3b of the main text, respectively.

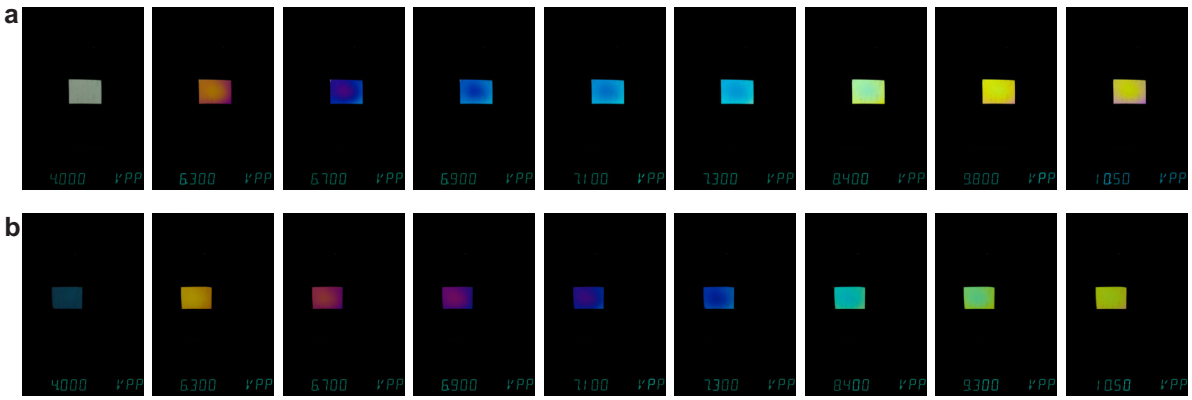

Figure S11: **Photograph of device** (a) Without the plasmonic nanostructure. (b) With the plasmonic nanostructure.

The inhomogeneities over the device originate mainly from the coating inhomogeneities in the liquid crystal cell. It can be seen that the plasmonic nanostructure enables the generation of a more saturated green compared to the liquid crystal cell alone, as predicted by modeling and in the transmission spectral. The exact nature of the colors as well as the voltages corresponding to the colors are deviated compared to simulations and transmission measurements due to the spectral distribution of the illumination (LED based) and the image sensor in the camera. For quantitative color analysis we refer to the CIE color plots in the manuscript.

References

(1) Duempelmann, L.; Luu-Dinh, A.; Gallinet, B.; Novotny, L. Four-Fold Color Filter Based on Plasmonic Phase Retarder. *ACS Photonics* **2016**, *3*, 190–196.

(2) Quaranta, G.; Basset, G.; Martin, O. J. F.; Gallinet, B. Recent Advances in Resonant Waveguide Gratings. *Laser Photonics Rev.* **2018**, *12*, 1800017.

(3) Johnson, P. B.; Christy, R. W. Optical-Constants of Noble-Metals. *Phys. Rev. B* **1972**, *6*, 4370.

(4) Christ, A.; Martin, O. J. F.; Ekinci, Y.; Gippius, N. A.; Tikhodeev, S. G. Symmetry Breaking in a Plasmonic Metamaterial at Optical Wavelength. *Nano Lett.* **2008**, *8*, 2171–2175.